35th International Electric Vehicle Symposium and Exhibition (EVS35)
Oslo, Norway, June 11-15, 2022

Self-Reconfigurable Battery Lifetime Management in EV Application

Jerome Blatter[1], Remy Thomas[1], Vincent Heiries[2], Ghislain Depesse[2]
[1]*Univ. Grenoble Alpes, CEA Liten, France*
[2]*Univ. Grenoble Alpes, CEA Leti, France*
name.lastname@cea.fr

Executive Summary

Due to factory production discrepancies and various operating conditions, cells integrated in conventional battery systems are not similar. In a static serial connection, the weakest cell always limits the battery pack capacity. Self-reconfigurable batteries (SRB), where semiconductor switches allow cells to be connected or bypassed dynamically, are used to by-pass the weakest cell and so use the full battery capacity at any time. The in-line configuration even allows direct generation of AC current without any power converter. This paper proposes a lifetime management strategy for SRB generating AC current. A full battery cell model including ageing mechanisms is used to perform the minimization of the SRB capacity losses with the aim of demonstrating the SRB capabilities in terms of lifetime extension in the EV application. The performance analysis of the strategy is achieved through simulation of the SRB using a standardized vehicle driving cycle at various Depth of Discharge and State of Heath. A whole battery life simulation allows estimating a battery lifetime extension of 40.6%.

Keywords: battery management, optimization, battery ageing, EV, simulation

1 Introduction

Electric battery vehicle (EV) seems to be the most promising solution to address the critical issues of replacing the actual fleet of combusting engine vehicle to contain the climate change. Lithium-ion battery are the most advanced battery technological solution for this due to its features: high energy and power density, long service life, low self-discharge and a market established technology. Unfortunately, Lithium-ion battery must operate under strict conditions. Especially each battery cell must be within the safe voltage range. Battery Management System (BMS) are used to supervise these conditions and correct some cell dispersions dues to factory production discrepancies and various operating conditions. These dispersions even appear between identical, brand-new cells from the same batch [1] and increase with the battery pack ageing [2]. In a traditional battery pack, cells are statically connected in series and in parallel to comply with voltage, current and capacity requirement. Additionally, the BMS frequently only correct the coulometric efficiency dispersion during battery charge. As a consequence, the weakest cell increasingly limits the entire battery pack capacity during discharge [3].
Self-reconfigurable batteries (SRB) are more advance battery architecture allowing inline reconfiguration of the overall cell layout based on the requested battery pack output voltage and the cell's state by using switches [4]. Therefore, an individual cell control taken into account the battery pack cell inconstancy is possible, and the battery pack is no more limited by the weakest cell. The individual cell control can even be used to find a cell control strategy that improve the battery lifetime. Significant lifespan improvements can be obtained by using SRB with optimal control. A lifetime extension of 16% is reached in [5] were

an optimal energy management is performed. Thus, the lifetime extension is an indirect consequence of this strategy. Therefore, this article aim to find a strategy optimizing the battery capacity loss which has a direct effect on the battery lifetime. This article is in continuation with the work presented in [6] where a optimal capacity loss strategy framework is introduced. The performance analysis is made on constant power battery discharge simulation with a low Depth of Discharge (DoD) of 25% and show a lifetime extension of 54%. The objective of this work is to show the SRB lifetime extension capabilities in the EV application by using this framework. Therefore, performance analysis of the optimal control strategy is done on SRB simulation using a power profile generated with the Worldwide harmonized Light vehicles Test Procedures (WLTP) cycle and using a simplified electric car motor model. Additionally, several batteries DoD are analysed by simulating SRB with profile of different length by using a different number of consecutive WLTP cycles. The SRB architecture used in this study is presented in [7] and is illustrated on Fig. 1. This architecture performs an inline reconfiguration of cells connected in series and allows the generation of a staircase sinusoidal voltage for one phase of an electric motor. In the same way, this SRB is capable of charging from the power grid without the need of an additional power converter. The individual cell control can be performed by acting on the proportion of time each cell is connected during the AC periods.

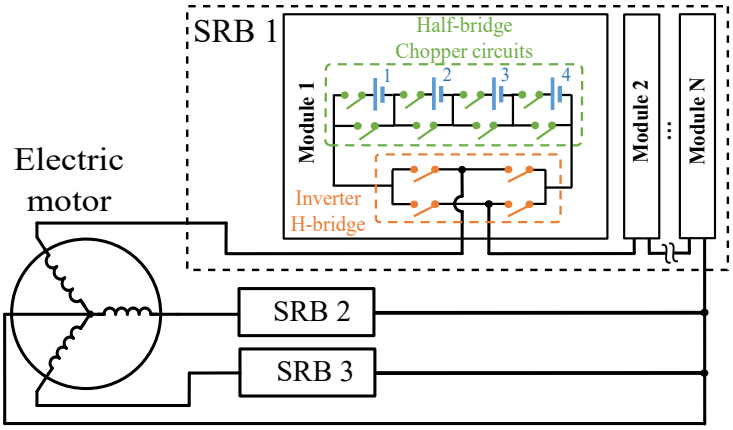

Figure 1: SRB hardware architecture for an electric vehicle usage

This paper is organized as follows. In section 2, the battery model used for this study is presented. It includes an electrical model and Li-ion cell-ageing model based on the battery cell model used in [8].In addition, this section presents the thermal model and the individual cell control model of the SRB. Section 3 formulates the process to get the power profile from the WLTP driving cycle with a simplified electric car motor model. Section 4 reminds the capacity loss optimization framework of [6]. Section 5 presents and analyses simulations results of the SRB at several DoD and ageing progress. Moreover, these simulations results are combined to reach a whole life SRB simulation to estimate the lifetime extension. Finally, section 6 concludes the paper.

2 Battery Model

This section underlines the battery cell model and the individual cell current model used in [6]. The first part of this section presents the cell behaviour according to the current flowing through the cell i_{cell}. Some modifications have been provided in comparison with [6]. Notably, heat exchange between cells and calendar ageing are added. Then, the second part describes the individual current repartition between cells of the SRB depending on the desired output AC signal and the system control vector u.

2.1 Battery cell model

The definition used for State of Charge (SoC), State of Health (SoH) and C_{rate} of a battery cell are given in Eq. (1) to (3).

$$SoC(t) = 100 - \frac{100}{3600(Q_{bol} - Q_{loss}(t))} \int_0^t i_{cell}(\tau)\, d\tau \tag{1}$$

$$SoH(t) = 100\, \frac{Q_{bol} - Q_{loss}(t)}{Q_{bol}} \tag{2}$$

$$C_{rate}(t) = i_{cell}(t)/Q_{nom} \tag{3}$$

with Q_{loss} the cell capacity loss since the beginning of life, i_{cell} the current circulating through the cell, Q_{nom} the cell nominal capacity provided by the manufacturer and Q_{bol} the measured cell capacity at beginning of life. We introduce an initial capacity dispersion model of the cells in the battery pack by a normal distribution of Q_{bol} around Q_{nom}.

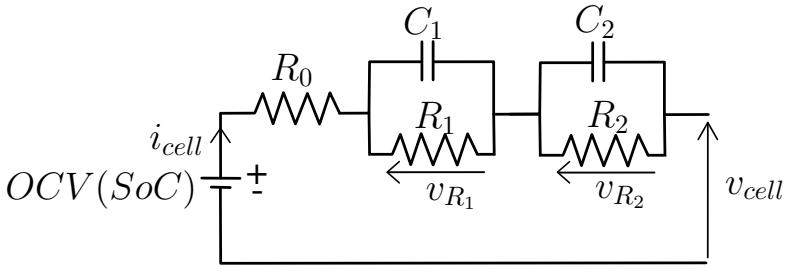

Figure 2: 2-RC Thevenin Electrical Equivalent Circuit model

The voltage behaviour of one cell is modelled with a 2-RC Thevenin model (Fig. 2) with an empirical parametrization of $R_1C_1 = 10s$ and $R_2C_2 = 100s$ in our uses case [8]. The impedances R_j, $j \in \{0, 1, 2\}$ are variable parameters regarding T, SoC, C_{rate} and SoH. The cell impedances are corrected using a multidimensional cartography obtained by hybrid pulse power characterization at different ageing progression [8, 4]. The related thermal power is obtained with the joule effect of the impedances R_j (4) [9]. Reversible heat generation can be ignored [2].

$$P_{th} = R_0\, i_{cell}^2 + \frac{v_{R_1}^2}{R_1} + \frac{v_{R_2}^2}{R_2} \tag{4}$$

In this work, it is assumed that the battery cell are mounted side by side in the battery containing n cells. Thus the battery cell temperature T follows the heat diffusion model (5) with a convection rate with the exterior h_{ext} and a conduction rate from one cell to the two neighbouring ones h_{trans}. C_p is the cell calorific capacity.

$$C_p\, \dot{T_j} = P_{th,\,j} - h_{ext}\,(T_j - T_{ext}) - h_{trans}(2\,T_j - T_{j-1} - T_{j+1}), j \in \{1 \cdots n\} \tag{5}$$

Equation (6) represents the capacity loss model of one cell [8]. It combines the degradation function law due to the battery cell cycling $\dot{Q}_{loss,\,cyc}$ (7) and the degradation due to the calendar ageing $\dot{Q}_{loss,\,cal}$ (8). The ageing speed of the calendar and cycling degradation function is adapted with the respective empirical function J dependent of the cell SoC, T and C_{rate}. The respective calendar and cycle ageing A and m are experimental fitted coefficients. An accelerated ageing protocol and a continuously cycling protocol of several cells at different T, SoC and C_{rate} is used to determine the parameters of the model.

$$\dot{Q}_{loss} = \dot{Q}_{loss,\,cyc} + \dot{Q}_{loss,\,cal} \tag{6}$$

$$\dot{Q}_{loss,\,cyc} = \frac{J_{cyc}(C_{rate}, T, SoC)}{(1 + A_{cyc}\, Q_{loss})^{m_{cyc}}}\ |i_{cell}| \tag{7}$$

$$\dot{Q}_{loss,\,cal} = \frac{J_{cal}(T, SoC)}{(1 + A_{cal}\, Q_{loss})^{m_{cal}}} \tag{8}$$

2.2 SRB individual cell current model

The SRB voltage is generated by controlling the number of cell connected in series. As a result, the SRB output voltage V_{pack} is a staircase waveform as represented in Fig. 3. The SRB output current i_{pack} is defined from the power profile to follow. Indeed, the SRB follows a reference voltage V_{ref} (9) while supplying a current i_{pack} (10). Therefore, the right amount of cell is needed to perform the voltage waveform and only the current repartition between the SRB cells is adjustable. This current distribution is controlled by choosing the right connection rate for each cell during one or more electrical periods, while ensuring an average connection rate sufficient to provide the desired output voltage.

$$V_{ref}(t) = \sqrt{2}\, U_{rms}(t) \sin(\theta(t)) \tag{9}$$

$$i_{pack}(t) = \sqrt{2}\, I_{rms}(t)\ \sin(\theta(t) + \phi(t)) \tag{10}$$

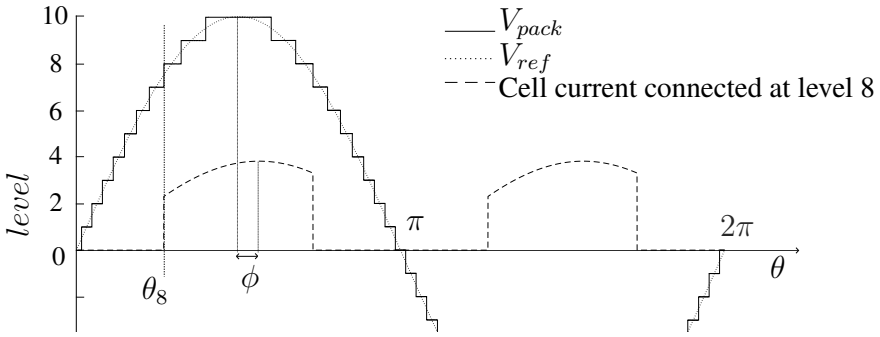

Figure 3: Staircase waveform generated by SRB

with U_{rms} the desired output rms voltage, I_{rms} the rms current, θ the signal phase and ϕ the current phase-shift compared to the SRB output voltage.
The rest of this section presents the average current model established in [6] to simplify the SRB model. The objective of this simplification is to have a cell current model that only depends on the system control vector u, U_{rms}, I_{rms}, ϕ and v_{cell} in order to reduce the model complexity concerning the resolution of the optimal solution. The average current flowing through a cell is simplified using (11).

$$i_{cell}(t) = i_{av}(t)\,\mu_{cell}(t) \tag{11}$$

with i_{av} the average current over all cells in one period (12). The system control vector u reflects the cell utilization rate. This vector is defined in (13) with n the number of cells in the battery pack.

$$i_{av} = \frac{1}{\pi \cdot n} \sum_{j} \int_0^{\pi} i_{cell,\,j}(\theta) d\theta \tag{12}$$

$$u = \left(\mu_{cell,\,1} \cdots \mu_{cell,\,j} \cdots \mu_{cell,\,n}\right)^T \tag{13}$$

An approximation of i_{av} can be done by considering the use of AC signal. Thus, i_{av} can be directly computed with (12) from U_{rms}, I_{rms}, ϕ and v_{cell}. An example of the current flowing through a cell connected at the eighth level is represented in Fig. 3. Therefore, the average current of this cell can be calculated by using Eq. (12).

It is necessary to constrain the mean value of the μ_{cell} to one in order to respect the amount of capacity consumed during the AC voltage periods. Furthermore, μ_{cell} dispersion must be limited to the maximal dispersion that the SRB is capable to deal with ([10]). A useful dispersion indicator is the stochastic variance. Thus, μ_{cell} variance must be kept smaller than $\mu_{var\,max}$ the maximal variance that the SRB is capable to handle, and must be limited within a lower bound (lb) and an upper bound (ub).
Eq. (14) summarizes all constraints on μ_{cell}.

$$\mathbf{C}(u,t) = \begin{cases} \underset{j}{\text{mean}}(\mu_{cell,\,j}) = 1,\ j \in \{1 \cdots n\} \\ \mu_{cell}(t) \geqslant \mu_{lb}(t) \\ \mu_{cell}(t) \leqslant \mu_{ub}(t) \\ \underset{j}{\text{var}}(\mu_{cell,\,j}(t)) \leqslant \mu_{var\,max}(t) \end{cases} \tag{14}$$

Finally, similarly to the calculation of i_{av}, an average power can be computed for joule effect associated to R_0 :

$$i_{av\,square} = \frac{1}{\pi \cdot n} \sum_{cell} \int_0^{\pi} i_{cell}^2(\theta) d\theta \tag{15}$$

3 Power profile

The objective of this section is to obtain the profile of $U_{rms}(t)$, $I_{rms}(t)$ and $\phi(t)$ of one motor phase supplied by one SRB from the WTLP driving cycle. The first step consists in the calculation of the mechanical equation of the EV motor. The power consumption $P(t)$ of the EV is obtained from the

WLTP vehicle speed $\mathrm{v}(t)$ by using Newton law (16) and the parameters in Tab.1. The electric motor speed ω and torque τ is obtained with respectively (18) and (19).

$$P(t) = \mathrm{v}(t)(m_e\dot{\mathrm{v}}(t) + C_r\, m\, g + \frac{1}{2}\rho_{air}\, SC_x\mathrm{v}(t)^2) \tag{16}$$

$$m_e = m + \frac{1}{R_{wheel}}(J_{motor}N^2 + n_{wheel}\, J_{wheel}) \tag{17}$$

$$\omega(t) = \frac{\mathrm{v}(t)}{R_{wheel}}N \tag{18}$$

$$\tau(t) = P(t)/\omega(t) \tag{19}$$

The second step consists in the calculation of the electrical equation of the EV motor. Therefore, the simplified synchronous electric machine model represented in Fig. 4 is used. It is assumed that the EV motor used an autopilot control (i_d = 0 A), i.e. the electromotive force $\left\|\vec{E}\right\| = k\,\omega$ is collinear to the motor current $\left\|\vec{I}\right\| = I_{rms}$. The current consumed to generate the induction field is ignored. Then, the assumption is done that the motor control switch from a constant flux control to a constant voltage control at $\mathrm{v} = v_{deflux}$.

Finally, in the constant flux mode, the profile is computed with $I_{rms}(t) = \frac{\tau(t)}{3\,k}$ and $k = k_{cst}$. In the constant voltage mode, the profile is computed with $P(t)/3 = k\,\omega\, I_{rms}$ and $U_{rms} = U_{max}$. $P(t)$ and $\tau(t)$ are divided by three because only the profile of one electric phase is considered. The maximal recovery current during the vehicle braking is limited to $I_{max,\,charge}$.

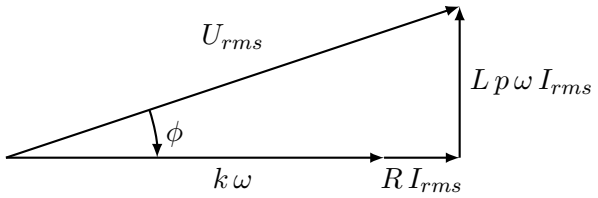

Figure 4: Fresnel diagram of an electric motor with autopilot control.

Table 1: EV parameters partly inspired by the Renault Zoé

	Values	Description
C_r	0.0111	Rolling friction coefficient
g	9.81 m/s^2	Acceleration of gravity
ρ_{air}	1.225 kg/m^3	Air density
SC_x	0.75 m^2	Drag area
m	1468 kg	Vehicle mass
n_{wheel}	4	Number of wheel
R_{wheel}	0.31 m	Wheel radius
J_{wheel}	8 kg/m^2	Wheel inertial
J_{motor}	0.25 kg/m^2	Motor inertial
N	10	Gear ratio
R	0.1 Ω	Motor equivalent electric resistance
L	0.48 mH	Motor equivalent electric induction
p	2	Motor poles pairs
v_{deflux}	40 km/h	Car speed from which the motor flux decrease
k_{cst}	0.6 Nm/A	Motor coefficient in constant flux mode
$I_{max,\,charge}$	63 A	Maximal rms breaking current
U_{max}	230 V	Maximal motor voltage

4 Optimisation framework

This section reminds the optimization problem formulates in [6] to optimize the SRB lifetime. Therefore, global optimization over a well-known profile that minimizes SRB capacity loss (20) respecting the SRB dynamic and its limits is performed. The SRB capacity loss is defined with the following expression $Q_{loss\,pack} = \underset{j}{\text{mean}}(Q_{loss,\,j})$, $j \in \{1 \cdots n\}$.

Minimize the cost function :

$$\min_{u(t)} \mathbf{J} = \min_{u(t)} \int_0^{t_f} t^2 \; Q_{loss,\,pack}(t)^2 \, dt \tag{20}$$

Subject to :

$$\dot{x}(t) = f(x(t), u(t), I_{rms}(t), U_{rms}(t), \phi(t)) \tag{21}$$

$$2.5 \leqslant \; v_{cell,\mathrm{j}}(x,t) \leqslant 4.2, \; j \in \{1 \cdots n\} \tag{22}$$

$$\mathbf{C}(u,t) \tag{23}$$

with $\mathbf{J}$ the cost function that must be minimized, t the time variable, x the system's state and f the dynamic system differential function. Thus, x is the combined state of every cell in the SRB, and it is defined as follows: $x = \left(\cdots SoC_j \cdots v_{R1,j} \cdots v_{R2,j} \cdots Q_{loss,j} \cdots T_j \cdots\right)^T$ where $j \in \{1, \cdots, n\}$.
u is the control vector defined in (13) witch control the average cell current submitted to the constraints (14).
f is defined by the combined dynamic of every cell model presented in subsection 2.1 and the average current model of the SRB in subsection 2.2. In addition, f also depends on the power profile presented in Section 3.
In order to return an easier to solve problem, (20) is a quadratic expression and has a weighting that increase with time.
For all batteries packs using Li-ion cells, voltage limits of every cell must be respected. This is included in the optimization problem with the inequality constraint (22).
Finally, this problem is solved with numeric methods. A direct multiple shooting method combined with a sparse matrix interior-point algorithm is used [11]. Discretization is performed by solving linear time-variant system for the computation of SoC, T and v. Q_{loss} is solved by performing the Euler method because the time step is chosen small compared to the other four variables.

5 Simulation results

Due to the complexity to solve optimization problem with high dimension, the battery pack chosen for the simulation only uses 15 Li-ions cells with $Q_{nom} = 2.9$A.h. We assume that the simulation is sufficient in order to deduce the optimal solution of a SRB using a higher number of cells. Therefore, it is necessary to adapt the power profile to the maximal output voltage and the capacity of the SRB using $n = 15$ cells: $U_{rms}(t)$ is normalized so that $\max_t(U_{rms}(t)) = \frac{n \cdot v_{cell,\,min}}{\sqrt{2}}$V with $v_{cell,\,min} = 2.5$V and I_{rms} is normalized so that the battery can perform 10 consecutive WLTP driving cycles without reaching the minimal voltage at battery begin of life (approximatively 230 km of autonomy). The resulting power profile use for the simulation is represented on Fig. 5.
The battery cell model is based on Nickel Manganese Cobalt (NMC) 18650 cell with graphite anode [8]. Additionally, the battery pack starts to be simulated with a normal distribution for cell's Q_{bol} and R_0, with a standard deviation of respectively 1% and 6% [2]. Battery cell numeration is in the ascending order of the cell's Q_{bol}.

5.1 SRB capacity loss gain

This subsection presents optimization simulation results of the power profile using the SRB at different levels of $DoD_{pack} = 1 - mean(SoC_j)$ and $SoH_{pack} = \underset{j}{\text{mean}}(SoH_j)$, $j \in \{1 \cdots n\}$. Simulations start with an initial SoC for every cell at 90%. This saves us to deal with the upper voltage limitations. Thus, there is no need to formulate assumption of a car breaking recovery energy management at high value of SoC. In addition, the SRB discharge is followed by a constant power charge at $V_{rms} = \frac{2.5\,n}{\sqrt{2}}$V and $I_{rms} = -3$A that bring the battery cells SoC back to 90%. Thus, the SRB power profile is composed of a variable number of consecutive WLTP profile followed by the constant power charge.

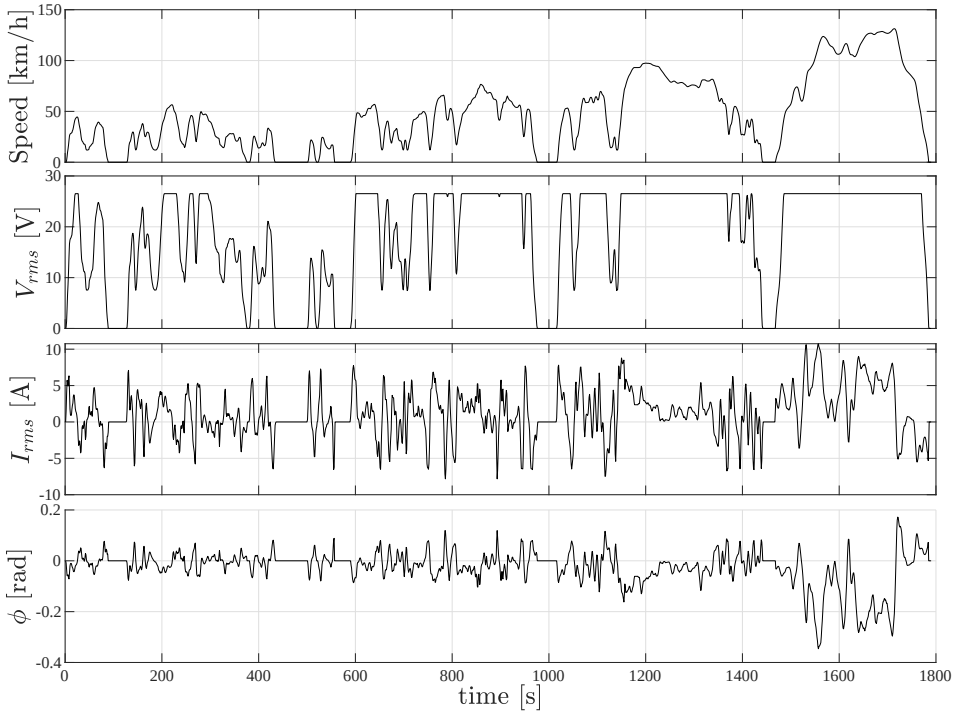

Figure 5: Power profile

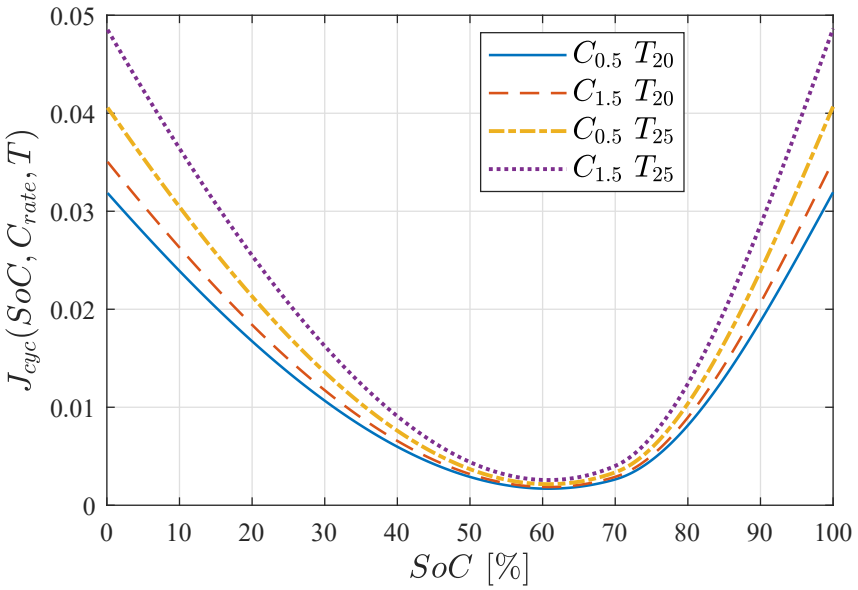

Figure 6: Cycling ageing speed function

To evaluate the performance of the optimal solution, a reference simulation is performed in parallel with exactly the same SRB and initial conditions as the simulation using the optimal solution in terms of SoC, T, v_{R_i} and Q_{loss}. However, the reference simulation is performed with no specific cell control and the cells are used in an equalized manner : $\mu_{cell,j} = 1,\ \forall j \in \{1 \dots n\}$. So, each cell endure the same average current similar to a traditional battery pack with a fixed series connection.
An example of the reference simulation is represented on Fig. 7a. This figure shows the simulated v_{cell}, SoC, T and μ_{cell} at 100% of SoH_{pack} and 2 consecutive WLTP cycles resulting in a DoD_{pack} of 27%. v_{cell}, SoC and T present some dispersions due to the initial dispersion of Q_{bol} and R_0.
The simulation of the SRB using a control strategy obtained by solving the optimization problem stated in section 4 and using the same initial condition and profile is represented on Fig. 7b. It can be observed through the behaviour of μ_{cell} that, the optimization is performed by using some cells at a higher rate

during the entire profile. As a consequence, these cells are submitted to a greater current resulting to a deeper discharge and higher cell temperature. This is possible by the fact, that the number of cells in the SRB is chosen to respect the output voltage when the cells are at minimum voltage as in traditional battery pack. That means, the SRB only needs some cells when the SoC is high to provide the output voltage.
The performance of this optimal simulation is observable on Fig. 8 which exhibits a comparison of the battery capacity loss evolution along time between the two simulations (100% of SoH and with a profile of 2 consecutive WLTP cycles followed by a constant power charge). The optimization allows reducing by 31% the total capacity loss compared to the reference simulation. This benefit is explainable by the cycling ageing behaviour illustrated in Fig. 6 representing the cycling ageing speed J_{cyc} of one cell in function of SoC for two representatives values of C_{rate} and T. The cell degradation is mainly caused by cycling at high value of SoC, and so ageing gain is obtained by reaching as soon as possible an optimal SoC value around 60% as shown on Fig. 7b with the SoC_{cell} behaviour.

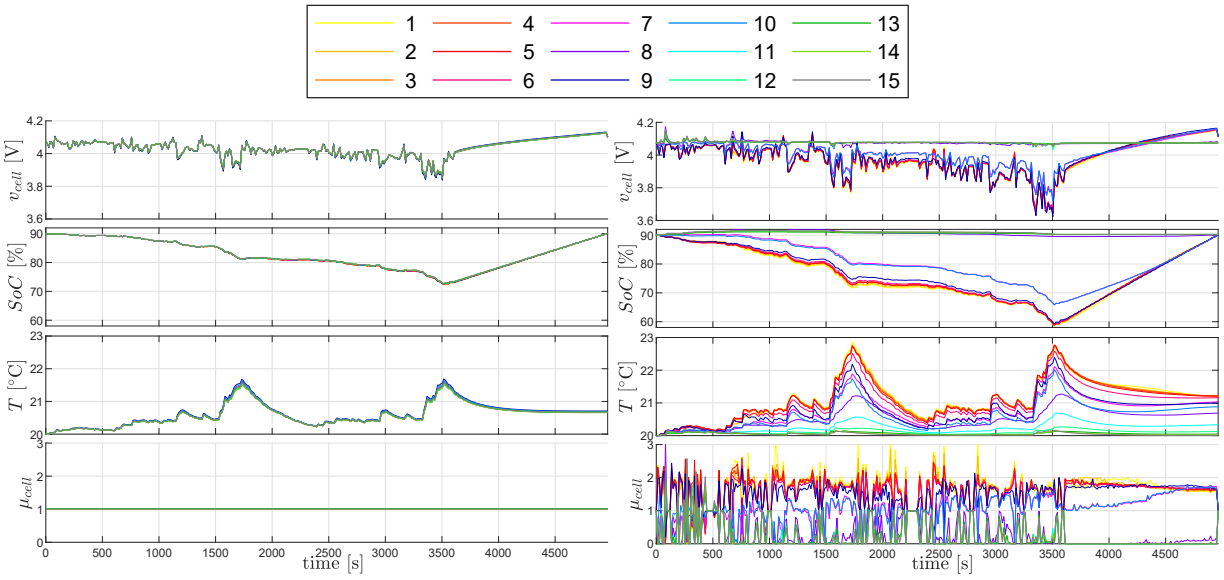

(a) Reference Simulation

(b) Simulation using the optimisation framework

Figure 7: SRB simulation at 100% of SoH and with a profile of 2 consecutive WLTP cycles followed by a constant power charge

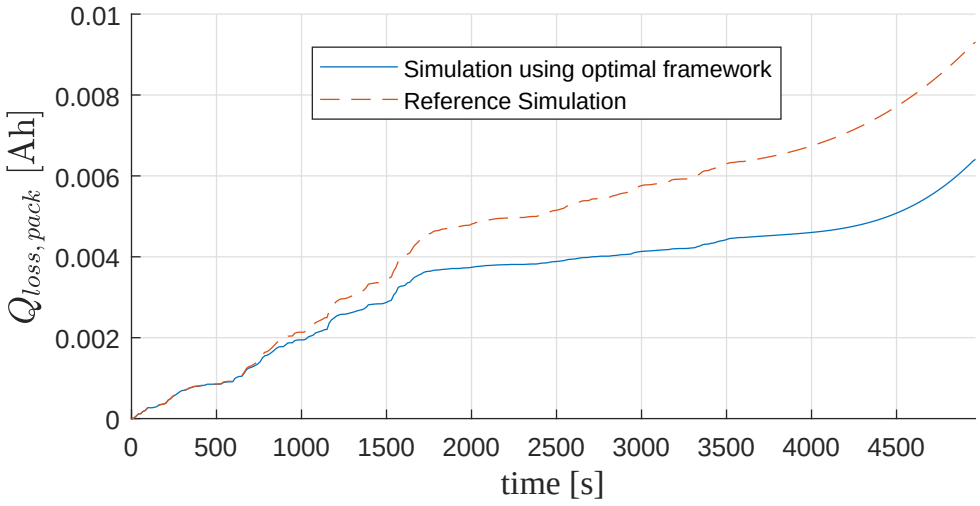

Figure 8: SRB capacity loss comparative between the reference and the optimization at 100% of SoH and with a profile of 2 consecutive WLTP cycles followed by a constant power charge

Finally, the capacity loss gain of the simulations using optimal control at different value of SoH_{pack} and DoD_{pack} are summarized on Tab .2. The different value of SoH_{pack} are obtained from a SRB which has cells aged at the same amount of $Q_{loss,\,j} = Q_{bol,\,pack}\,(1 - SoH_{pack})$. It can be observed that a great capacity loss gain can be obtained with the optimal control when the DoD_{pack} is low because it is possible from the SRB to bring faster some cell in the SoC zone with the lower ageing speed and not to use the other ones. However, when the DoD_{pack} is higher, it is more difficult not to use some cell and to have the other in the optimal SoC zone.

Table 2: DoD_{pack} and capacity loss gain of the optimal solution in comparison with the reference for simulation using different power profile length and different SoH_{pack} (Simulation start with DoD_{pack}=10%)

SoH	100%		95%		90%		85%	
Num. WLTP	DoD	Gain	DoD	Gain	DoD	Gain	DoD	Gain
1	19%	22%	20%	23%	20%	22%	20%	24%
2	27%	31%	28%	30%	30%	30%	31%	29%
3	36%	10%	38%	8%	39%	8%	41%	9%
4	45%	8%	47%	8%	49%	8%	52%	7%
5	54%	7%	57%	5%	59%	7%	63%	8%
6	64%	6%	67%	8%	70%	8%	74%	6%

5.2 Lifetime extension estimation

To estimate a lifetime extension of the optimal control strategy in comparison to the reference control, the whole SRB life can be simulated by cycling profiles of various DoD until a SoH threshold is reached. Between each cycle, the SRB SoC, v_{Ri} and T are reset to the initial condition. Only Q_{loss} are transferred from a cycle to the next one. Each profile length is uniformly randomly composed of 1 to 6 consecutive WLTP driving cycles for varying the DoD.
However, optimization over the whole lifetime is not possible due to the high dimension of the optimization problem. Suboptimal simulation can be performed by reusing the optimal control sequences $u(t)$ obtained from the optimization performed for the simulations whose results are summarized in Tab. 2. For each cycle, the optimal solution with the corresponding number of consecutive WLTP cycles and with the closest superior SoH is chosen.
In addition, to have cells that reach end of life at the same time, the SRB optimal control vector $u(t)$ is permuted between cells for each profile in such a way that $Q_{loss,\mathrm{j}},\ j \in \{1 \cdots n\}$ is equalized in long-term. Indeed, we have previously seen that the optimization is mainly based on the fact a that some cell reach faster the optimal SoC zone, and so the initial parameter dispersion between cell have a small effect on the capacity loss gain. Therefore, permuting some cells that have a high utilization rate with those having a low utilization rate between profile is an acceptable suboptimal solution.
In parallel, the reference simulation is produced by cycling exactly the same profile sequence until it reaches SRB's end of life and with $\mu_{cell,\,j} = 1,\ \forall j \in \{1 \ldots n\}$.

Fig. 9 displays SRB capacities of the reference simulation and the optimal control simulation during the whole lifetime with the previously mentioned protocol. If the SRB end of life is defined arbitrarily when the mean capacity value of the cells reach 2.32 Ah (80% SoH_{pack}), it can be seen that the reference simulation performs 40 kWh and the simulation using the optimal control 45 kWh. This represents a lifetime extension of 12.5%.

Knowing the benefits of the optimal control compared to reference control for SRB, it would be interesting to compare this result to conventional battery pack. The balancing capabilities of SRB experimented in [10] are so efficient that it can be assumed that the SRB is capable to extract the energy of all cells. The mean value of the cells capacities is then a good image of the battery pack capacity. On the other side, the conventional battery is limited by the weakest cell. We assume that the conventional battery capacity with exactly the same Li-on cell connected in series and using a DC/AC converter to provide the AC output signal, is represented by the cell with the lowest capacity in the SRB with the reference control. We also assume that the SRB with reference control and the conventional battery pack have the same ageing speed.
The conventional battery end of life is observed at 32 kWh. Finally, the SRB using the optimal strategy enables lifetime extension of 40.6% compared to the conventional battery.

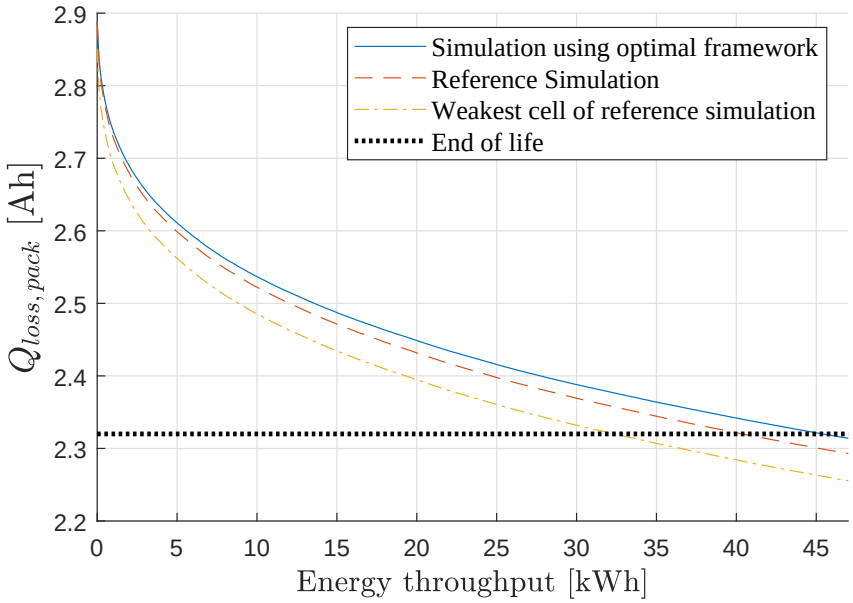

Figure 9: Mean cell capacity comparison between the reference simulation and simulation using the optimal control during the whole lifetime. The weakest cell capacity of the reference simulation is also plotted (graphique provisoire)

6 Conclusion

In a precedent work [6], a battery lifetime optimization framework for SRB generating AC waveform signal was presented. A performance analysis was achieved using simulation on simple constant power profile and exhibits a lifetime extension of 54%. This paper proposes to apply the same methodology for the EV use case through driving profile. Therefore, after reminding the battery model and the optimization framework, a simplified EV motor model is presented to generate the SRB power profile based on the WLTP driving cycle. This allows performing various optimization results at different DoD and battery ageing stages showing the SRB lifetime extension benefits. A battery lifespan extension estimation, performed by cycling profile of different length during the whole battery life, exhibits an improvement of 40.6% compared to an equivalent standard battery.
Furthermore, this work can be used to evaluate the performance and give some clues for the development of real time control as already performed in [12] with the development of a nonlinear Model Predictive Control (nMPC) achieving a 12.4% capacity loss reduction on one WLTP cycle.

Acknowledgments

The battery ageing model comes from the NENUFAR project (with partners Thales, Arkema, TTTech and University of Erlangen) supported by the European Union under the framework of the Clean Sky 2 program / GAM 945539 - .

References

[1] K. Rumpf, A. Rheinfeld, M. Schindler, J. Keil, T. Schua, and A. Jossen, “Influence of Cell-to-Cell Variations on the Inhomogeneity of Lithium-Ion Battery Modules,” *Journal of The Electrochemical Society*, vol. 165, no. 11, pp. A2587–A2607, 2018.

[2] S. Paul, C. Diegelmann, H. Kabza, and W. Tillmetz, “Analysis of ageing inhomogeneities in lithium-ion battery systems,” *Journal of Power Sources*, vol. 239, pp. 642–650, 2013.

[3] L. Lu, X. Han, J. Li, J. Hua, and M. Ouyang, “A review on the key issues for lithium-ion battery management in electric vehicles,” *Journal of Power Sources*, vol. 226, pp. 272–288, 2013.

[4] L. Komsiyska, T. Buchberger, S. Diehl, M. Ehrensberger, C. Hanzl, C. Hartmann, M. Hölzle, J. Kleiner, M. Lewerenz, B. Liebhart, M. Schmid, D. Schneider, S. Speer, J. Stöttner, C. Terbrack, M. Hinterberger, and C. Endisch, "Critical Review of Intelligent Battery Systems: Challenges, Implementation, and Potential for Electric Vehicles," *Energies*, vol. 14, no. 18, p. 5989, Sep. 2021.

[5] N. Bouchhima, M. Gossen, S. Schulte, and K. P. Birke, "Lifetime of self-reconfigurable batteries compared with conventional batteries," *Journal of Energy Storage*, vol. 15, pp. 400–407, Feb. 2018.

[6] J. Blatter, V. Heiries, R. Thomas, and G. Despesse, "Optimal lifetime management strategy for self-reconfigurable batteries," manuscript submitted for publication.

[7] R. Thomas, G. Despesse, S. Bacquet, E. Fernandez, Y. Lopez, P. Ramahefa-Andry, and L. Cassarino, "A high frequency self-reconfigurable battery for arbitrary waveform generation," *World Electric Vehicle Journal*, vol. 12, no. 1, pp. 1–12, 2021.

[8] A. Laurin, V. Heiries, and M. Montaru, "State-of-Charge and State-of-Health online estimation of Li-ion battery for the More Electrical Aircraft based on semi-empirical ageing model and Sigma-Point Kalman Filtering," in *2021 Smart Systems Integration (SSI)*, Apr. 2021, pp. 1–4.

[9] C. Forgez, D. Vinh Do, G. Friedrich, M. Morcrette, and C. Delacourt, "Thermal modeling of a cylindrical LiFePO4/graphite lithium-ion battery," *Journal of Power Sources*, vol. 195, no. 9, pp. 2961–2968, May 2010.

[10] R. Thomas, F. Lehmann, J. Blatter, G. Despesse, and V. Heiries, "Performance analysis of a novel high frequency self-reconfigurable battery," *World Electric Vehicle Journal*, vol. 12, no. 1, pp. 1–12, 2021.

[11] A. Rao, "A Survey of Numerical Methods for Optimal Control," *Advances in the Astronautical Sciences*, vol. 135, Jan. 2010.

[12] J. Blatter, V. Heiries, R. Thomas, and G. Despesse, "Nonlinear model predictive control for lifetime extension of self-reconfigurable batteries," manuscript submitted for publication.

Presenter Biography

Jerome Blatter received an engineer Master degree from ENSEM, Nancy, France, in 2019. He is currently working toward the PhD degree at the EEATS doctoral school, Grenoble Alpes University, France. His research interests include battery management system and self-reconfigurable battery.

Remy Thomas received a master's degree in electrical and electronics engineering from the French School Phelma of Grenoble Institute of Technology, France, in 2008. He joined the CEA-LITEN Laboratory in 2010 as research engineer to work on Battery Management Systems as well as Fuel Cell Management Systems, and more specially on real-time embedded systems for which he has developed a good expertise in both software and hardware.

Vincent Heiries received the Master graduation degree from ENAC (French National School of Civil Aviation) in 2003 and the PhD degree in signal processing and digital communications from ISAE (Supaero). He has worked several years with THALES Space in the field of navigation satellite systems (GPS, GALILEO). Since 2012, he has been working at CEA and his research activities are mainly focused on signal processing applied to fault detection in electrical systems, and battery management systems. He is the author or co-author of more than 20 publications and main inventor or co-inventor of 12 patents.

Ghislain Despesse graduated (MS degree) in electrical engineering from Ecole Normale Supérieure de Cachan (ENS) in 2002 and he received his Ph.D. Degree in microelectronics from the National Polytechnic Institute of Grenoble (INPG), France, in 2005. He joined the CEA-LETI Laboratory in 2005. He was involved in the development of vibrational energy harvesters using electrostatic or piezoelectric conversion principle. He is implicated for ten years in the development of Battery Monitoring Systems (BMS) including inverter functions for the electrical vehicle and others applications. He contracted a good experience in electrostatic and piezoelectric transduction mechanisms to sense, actuate or to convert energy. He has published 78 papers in refereed journals and conferences. He holds 81 patents in the fields of energy scavenging, energy conversion and power management. He received his ability to drive research in 2017.